



A backward pre-stressing algorithm for efficient finite element implementation of *in vivo* material and geometrical parameters into fibril-reinforced mixture models of articular cartilage

Seyed Shayan Sajjadinia ^a, Bruno Carpentieri ^{a,*}, Gerhard A. Holzapfel ^{b,c}

^a Faculty of Computer Science, Free University of Bozen-Bolzano, Bozen-Bolzano, 39100, Italy

^b Institute of Biomechanics, Graz University of Technology, Stremayrgasse 16/2, Graz, 8010, Austria

^c Department of Structural Engineering, Norwegian University of Science and Technology (NTNU), Trondheim, Norway

ARTICLE INFO

Keywords:

Simulation

Inverse finite element analysis

Articular cartilage mixtures

Pre-stress

ABSTRACT

Classical continuum mechanics has been widely used for implementation of the material models of articular cartilage (AC) mainly with the aid of the finite element (FE) method, which, in many cases, considers the stress-free configuration as the initial configuration. On the contrary, the AC experimental tests typically begin with the pre-stressed state of both material and geometrical properties. Indeed, imposing the initial pre-stress onto AC models with the *in vivo* values as the initial state would result in nonphysiologically expansion of the FE mesh due to the soft nature of AC. This change in the model configuration can also affect the material behavior kinematically in the mixture models of cartilage due to the intrinsic compressibility of the tissue. Although several different fixed-point backward algorithms, as the most straightforward pre-stressing methods, have already been developed to incorporate these initial conditions into FE models iteratively, such methods focused merely on the geometrical parameters, and they omitted the material variations of the anisotropic mixture models of AC. To address this issue, we propose an efficient algorithm generalizing the backward schemes to restore stress-free conditions by optimizing both the involving variables, and we hypothesize that it can affect the results considerably. To this end, a comparative simulation was implemented on an advanced and validated multiphasic model by the new and conventional algorithms. The results are in support of the hypothesis, as in our illustrative general AC model, the material parameters experienced a maximum error of 16% comparing to the initial *in vivo* data when the older algorithm was employed, and it led to a maximum variation of 44% in the recorded stresses comparing to the results of the new method. We conclude that our methodology enhanced the model fidelity, and it is applicable in most of the existing FE solvers for future mixture studies with accurate stress distributions.

1. Introduction

Finite element (FE) analysis provides a numerical tool for multiphasic modeling of the articular cartilage (AC). It is presumed that AC is formed by a combination of fibril-reinforced and non-fibrillar mixture coupled with a charged biphasic medium (Freutel et al., 2014; Halloran et al., 2012; Julkunen et al., 2013; Klika et al., 2016). The electrochemical behavior is necessary for biomechanical simulation of AC constituents (Quiroga et al., 2017; Sajjadnia et al., 2019), and it can pre-stress the solid matrix even in the absence of external loads at the beginning of the analysis. As FE models are mainly based on continuum mechanics, where typically a stress-free condition is assumed as the initial condition, the AC pre-stress can expand the FE mesh of the model

and ultimately extend the fiber bundles until it reaches equilibrium. Therefore, if the numerical analysis starts with the experimental configuration, such volume expansion will cause computational errors in the initial configuration getting a shape dissimilar to *in vivo* measurements (Wang et al., 2018). Although it is occasionally possible to guess a stress-free configuration, which would result in the initial *in vivo* condition by a forward FE analysis, it is challenging or even impossible to make such speculation for heterogeneous and large-scale models.

On the other hand, the complex constituents of cartilage are commonly modeled by the mixture theory (Truesdell and Toupin, 1960) in accordance with a relationship between the isotropic and anisotropic material fractions, which are functions of the geometrical parameters (Wilson et al., 2007). Therefore, even if the stress-free geometry of the

* Corresponding author.

E-mail address: bruno.carpentieri@unibz.it (B. Carpentieri).

FE models was available, these parameters could be altered non-physiologically by the pre-stress deformation. In other words, the issue of implementation of the initial *in vivo* conditions is not limited to geometrical parameters, and it also has an effect on the initial values of the material parameters of the mixture models.

It is, however, possible to determine the stress-free condition numerically or experimentally, as some methods have already been presented in the literature with applications in different fields of science, see, e.g., Fachinotti et al. (2008), Govindjee and Mihalic (1996), Huang et al. (2016) and Lu et al. (2007). In the context of biological pre-stressing, several techniques for different soft tissues have been suggested. Some of these approaches are based on the multiplicative split of the deformation gradient (Gee et al., 2010; Pierce et al., 2015; Weisbecker et al., 2014), which were also used in tissue growth and remodeling models (Ambrosi et al., 2019; Zahn and Balzani, 2016). Although these methods are robust, they may require a manipulation of the FE elements or the constitutive equations, which are not straightforward for some research groups working with commercial software packages. Other more sophisticated methods are also available for this purpose, see, e.g., Alastrué et al. (2007), Lu et al. (2007) and Olsson et al. (2006), which are built on different approaches, such as the opening-angle algorithms, inverse design analysis, etc., but they can find the initial conditions under very specific circumstances, such as specific constitutive or geometrical assumptions. Alternatively, the so-called fixed-point-based backward schemes can accurately find the stress-free geometry in a very straightforward manner, as they consider numerical models as black-box systems, and they perform the pre-stress algorithms by only the input and output geometrical values of these systems without manipulation of the background numerical equations (Leach et al., 2019).

In particular, for AC analysis, recently an efficient pre-stressing algorithm was proposed (Wang et al., 2018) based on the previous fixed-point-based backward displacement method (Bols et al., 2013). This algorithm was successfully applied to a patient-specific AC model, and while it was a step forward, their methods were completely geometry-based and did not take into account the important material variations due to the kinematic variations in the mixture models. Therefore, this limitation can be addressed by a new backward optimization algorithm with the capability of material optimization (MO) that can also optimize the stress-free states for these material parameters so that the FE models would start with the *in vivo* data after equilibrium.

The present study proposes a backward method with the aim of incorporating the *in vivo* initial conditions that can encompass both the geometrical changes and the kinematic-induced constitutive variations of the AC mixture models due to pre-stressing. As no modification of the element equations is required, we consider our algorithm as a pragmatic implementation method, applicable in most of the commercial FE solvers, which we hypothesize can highly affect the results of the AC mixture models in comparison to the results by the

conventional backward FE analysis. To study our hypothesis, an advanced multiphasic model was implemented in an unconfined compression simulation with and without MO. Besides, using another tensile test, we calibrated material models of AC before the implementation of the main simulation.

2. Materials and methods

2.1. Theoretical background

We first assumed that the capital letters signify the stress-free condition, while the superscript *REF* denotes the correspondence to the initial *in vivo* (reference) condition with pre-stress. The experimental parameters in this study were acquired from published *in vivo* data used in the healthy knee cartilage model of the former tissue-scale study (Sajjadinia et al., 2019).

In conventional FE codes, a forward simulation starts with the stress-free initial configuration with \mathbf{X} as the material coordinates of each point. When the pre-stress σ_0 is introduced inside an AC model, its structure deforms to the new configuration with \mathbf{x} as the updated geometry. At this stage, the model would reach the equilibrium condition, where the boundary conditions and the solid components resist this internal pressure, and following that, the main simulation can start. Therefore, if the analysis starts with the true *in vivo* configuration ($\mathbf{X} = \mathbf{X}^{REF}$), after the pre-stress equilibrium, the main simulation will begin with the geometrical error of $\mathbf{x} - \mathbf{X}^{REF}$ in the initial configuration.

In the conventional inverse problems of pre-stressing (Bols et al., 2013; Wang et al., 2018), the initial *in vivo* and stress-free configurations were assumed to be the known and unknown parameters, and the aforementioned forward analysis starts with the *in vivo* configuration. Next, the stress-free configuration is revised by an update function \mathbf{U} , and the forward analysis is iterated unless the maximum value of a residual function *maximum(r)* converges to a small number of ϵ , implying that the initial pre-stressed geometries closely match the *in vivo* observations (i.e., $\mathbf{x} \approx \mathbf{X}^{REF}$). As this method can only optimize the geometrical parameters, it is a geometry-based methodology, which can be implemented in each node of the FE models, as summarized in Algorithm 1, using the following update and residual functions

$$\mathbf{U} = \mathbf{X}^{REF} - \mathbf{x} \quad (1)$$

$$r = \|\mathbf{x} - \mathbf{X}^{REF}\|_2 \quad (2)$$

where $\|\cdot\|_2$ is the L^2 norm. This iterative procedure, however, is restricted to the nodal geometrical parameters, which may not be flawless in the mixture models.

Algorithm 1. Implementation of the geometry-based backward algorithm at each point to recover the pre-stress configuration.

1. Initialize the forward model with the initial *in vivo* data
2. while $\text{maximum}(r) > \epsilon$ do:
3. Perform a forward analysis by imposing the pre-stress σ_0 into the current configuration of the model \mathbf{X} to find the updated configuration \mathbf{x} after equilibrium
4. For each point do:
 5. $\mathbf{U} \leftarrow \mathbf{X}^{REF} - \mathbf{x}$
 6. $\mathbf{X} \leftarrow \mathbf{X} + \mathbf{U}$
 7. $r \leftarrow \|\mathbf{x} - \mathbf{X}^{REF}\|_2$
 8. end for
 9. end while

To clarify the limitation of [Algorithm 1](#), this study used an advanced validated multiphasic model ([Sajjadinia et al., 2019](#)), which was developed based on a number of publications ([Buschmann and Grodzinsky, 1995; Stender et al., 2012; Taffetani et al., 2014; Wilson et al., 2004, 2007; Wu and Herzog, 2000](#)), and particularly, the biphasic theory ([Mow et al., 1980](#)) was employed, which divides the AC components into the inviscid water and the (effective) solid parts. A permeability function then governs the interaction between both phases, and the Cauchy stress σ in AC is defined as

$$\sigma = \sigma^{EFF} - p\mathbf{I} \quad (3)$$

where p , σ^{EFF} , and \mathbf{I} are the fluid (or pore) pressure, the (effective) solid stress, and the unit tensor, respectively. When assuming the solid part as a constrained mixture of the non-fibrillar matrix σ^{MAT} , representing the proteoglycan effect, the tensile stress in the fibrillar network σ^{COL} , representing the anisotropic collagen effect, and the swelling (or osmotic) stress σ^{GAG} due to AC fixed-charged nature by microscopic glycosaminoglycan (GAG) chains, the solid stress can be formulated as

$$\sigma^{EFF} = \sigma^{COL} + \sigma^{MAT} - \sigma^{GAG} \quad (4)$$

with

$$\sigma^{COL} = \frac{\phi_0^S}{J} \sum_{l=1}^9 (\lambda^l \rho_C^l (E_0 + E_e \epsilon^l) \epsilon^l \mathbf{n}^l \otimes \mathbf{n}^l) \quad (\text{if } \epsilon^l > 0) \quad (5)$$

$$\sigma^{MAT} = \phi_0^S \frac{G_m (1 - \rho_0^{COL})}{J} \left[-\frac{\ln J}{6} \left(3\phi_0^S \frac{J \ln J}{(J - \phi_0^S)^2} - 1 - 3 \frac{J + \phi_0^S}{J - \phi_0^S} \right) \mathbf{I} + (\mathbf{F} \cdot \mathbf{F}^T - J^{2/3} \mathbf{I}) \right] \quad (6)$$

$$\sigma^{GAG} = \alpha_1 \left(\frac{1}{J} \right)^{\alpha_2} \mathbf{I} \quad (7)$$

Herein, $\sum_{l=1}^9 (\cdot)$ is the summation operator for 7 secondary and 2 primary fibrils at each point, α_1 , α_2 , G_m , E_0 , and E_e are material constants, \otimes and \cdot are the dyadic and inner products, \mathbf{n}^l , ϵ^l , ρ_C^l , and λ^l denote the direction, the logarithmic strain, the volume fraction, and the elongation

of the I -th fibril, respectively, while ϕ_0^S and ρ_0^{COL} are the initial values of the solid ϕ_0^S and the total collagen ρ_0^{COL} volume fractions, and J is the determinant of the deformation gradient \mathbf{F} , which is the partial differentiation of the deformed coordinates with respect to the undeformed coordinates, derivable by the solvers at each integration point. Some of the above material parameters can be updated for this anisotropic mixture model by their initial value and deformation of the model, i.e.

$$\mathbf{n}' = \frac{\mathbf{F} \cdot \mathbf{N}'}{\|\mathbf{F} \cdot \mathbf{N}'\|_2} \quad (8)$$

$$\phi = \frac{\phi_0}{J} \quad \text{if } \phi \in \{\phi_0^S, \rho_0^{COL}\} \quad (9)$$

As the values of these parameters can vary by the change of configuration in [Algorithm 1](#), if they again start with the in vivo values, the pre-stressed configuration will cause errors in the initial conditions of the main simulation afterward. The initial in vivo values for these material parameters can be obtained from the literature. Here, the following experimentally-based models were used ([Lipshitz et al., 1975; Rieppo, 2004; Shapiro et al., 2001; Wilson et al., 2007](#)):

$$\phi^S(\text{REF}) = 0.1 + 0.2z \quad (10)$$

$$\rho^{COL}(\text{REF}) = 1.4z^2 - 1.1z + 0.59 \quad (11)$$

where z is the normalized depth. Likewise, fibril bundles at the initial in vivo state are oriented in specific directions, as elaborated in a previous study ([Sajjadinia et al., 2019](#)), on the basis of experimental data ([Benninghoff, 1925; Wilson et al., 2004](#)). For illustrative purposes, the direction of one of the primary fibrils, as representative of the other fibrils, is displayed in [Fig. 1](#). Generally, all the in vivo data used in this study are based on the average experimental observations and they are, therefore, free of outliers.

Finally, for the implementation of the backward optimization algorithm, it was also assumed that the osmotic pressure is set to have the fixed value of σ_0 before the initial equilibrium of the pre-stress ([Wang et al., 2018](#)) such that upon reaching the pre-stress equilibrium, the osmotic pressure is allowed to increase with the volumetric change in the main simulation. Obviously, the stresses in the AC components are initially zero, except for the osmotic part, which results in the pre-stress

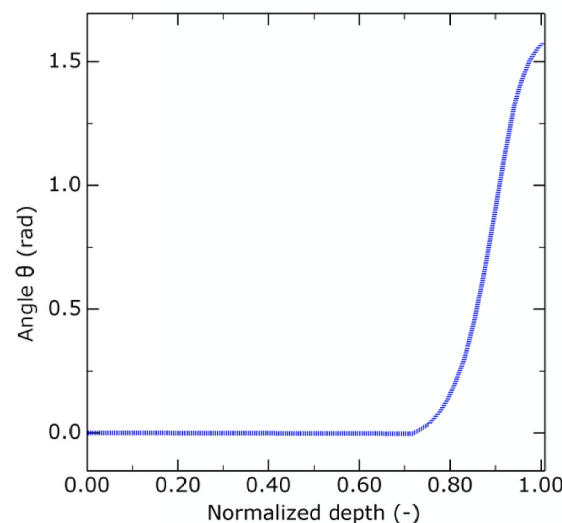
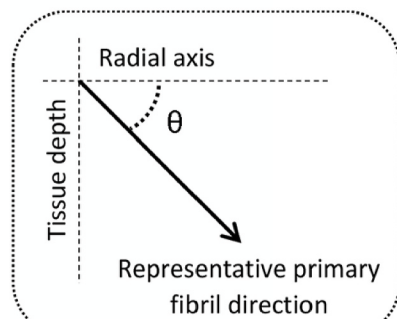


Fig. 1. Angle between the radial axis and a representative primary fibril θ at each location in the initial in vivo state ([Benninghoff, 1925; Wilson et al., 2004](#)).

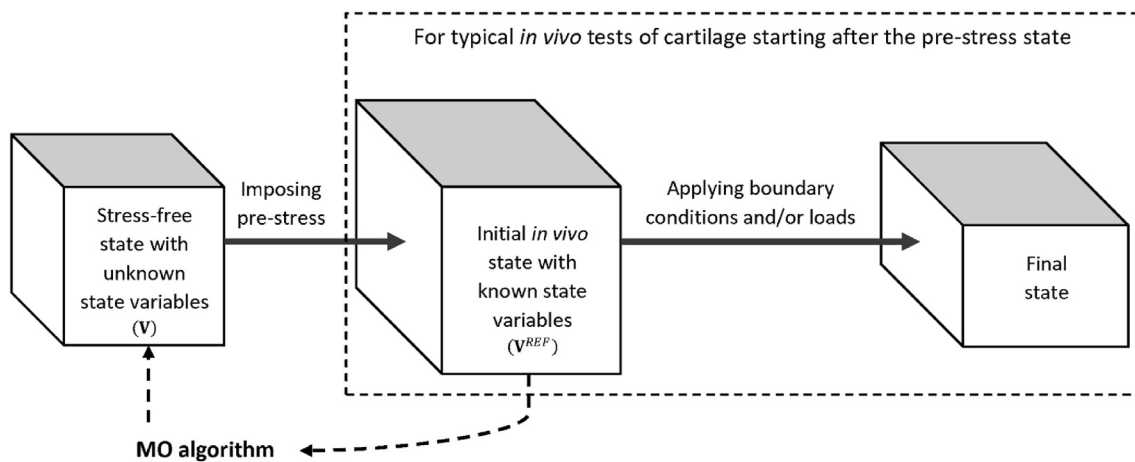


Fig. 2. Schematic of the MO algorithm role in different states of the simulations: at first, the problem is supposed to start within the stress-free state with unknown state variables, including both geometrical and material parameters. Then after imposing the pre-stress, the state variables are updated to their new values, which should match the initial conditions of typical *in vivo* tests, considering that experiments usually begin with the pre-stressed state. In order to find the values at the stress-free state, the MO backward algorithm can be employed that iteratively updates the initial guess of the state variables to reach the initial *in vivo* values. Once they are found, the main numerical analysis can then be implemented to simulate the experimental test.

$\sigma_0 = -\alpha_1 \mathbf{I}$, obtained by substituting the initial deformation, $\mathbf{F} = \mathbf{I}$, into eqs. (4)–(7).

2.2. Backward algorithm with MO

Due to the need to incorporate the changes in the material parameters, here [Algorithm 1](#) is extended to find the stress-free state of all the relevant parameters, including the material variables (i.e., \mathbf{N}^T , \emptyset_0^S , ρ_0^{COL}) and the geometrical parameters (i.e., \mathbf{X}). If \mathbf{V} denotes the stress-free states of these optimization parameters, by performing a forward pre-stress analysis, it should be updated to \mathbf{v} . Given \mathbf{V}^{REF} from the *in vivo* data, as the known values in the new algorithm, we chose \mathbf{V} as the unknown which results in \mathbf{v} converging to \mathbf{V}^{REF} . The algorithm is again based on iteratively updating the initial values until the convergence is achieved based on a residual function; however, this time rather than merely updating the geometrical parameters, all the state variables are updated, see [Fig. 2](#).

By defining the subscripts of A and R as the subsets of anisotropic material parameters and the remaining isotropic or geometrical parameters, the update function for the isotropic material and the geometrical parameters \mathbf{U}_R is defined by

$$\mathbf{U}_R = \mathbf{V}_R^{REF} - \mathbf{v}_R \quad (12)$$

which is clearly an extension to eq. (1), but it is an inappropriate definition for the anisotropic parameters, as these parameters are governed by their directional unit vectors, which are not independent of each other. Updating these dependent components separately is very challenging in large deformable bodies as they are also nonlinearly dependent on their exact directions in space. The most straightforward way to handle this issue is to calculate the updated anisotropic values in each iteration by an inverse FE analysis that eliminates the need to use the update function. On that basis, at each iteration, a FE analysis should be carried out for the same model but with the initial *in vivo* and updated

geometries as the initial and final conditions, respectively, which can be imposed onto this model via the displacement boundary conditions of $\mathbf{x} - \mathbf{X}^{REF}$ at each node, meaning that the inverse model simulates a mapping of $\mathbf{X}^{REF} \mapsto \mathbf{x}$ after each mapping $\mathbf{X} \mapsto \mathbf{x}$ in the forward analysis. This way, the updated values \mathbf{v}_{ANI} can be obtained by the calculated deformation gradient of this inverse model. Subsequently, the updated residual function is evaluated for all parameters by

$$r = \|\mathbf{v} - \mathbf{V}^{REF}\|_2 \quad (13)$$

Currently, several pre-stressing algorithms have been implemented and applied to other tissues that can encompass some of the material changes. Comparing to them, the major difference, beyond the constitutive equations, is the relationship that updates the relevant material parameters in each iteration, see, e.g., [Alastrué et al. \(2010\)](#) or [Grytz and Downs \(2013\)](#), who used the multiplicative decomposition of the deformation gradient to update the state of the fiber directions. Despite this, the variations in the material states in this study depend also indirectly on the deformation gradient through eqs. (8) and (9), rendering this algorithm conceptually similar to them.

In terms of implementation complexity, our MO algorithm complicates further the whole iteration process, considering that it requires access to the values of the deformation gradient at each integration point. Nonetheless, we do not consider this as a limitation because even our material model could not have been implemented without such access. It can also be implemented in most of the FE solvers through some custom coding without much efforts (e.g., refer to [Section 2.3](#)), comparing to even the highly pragmatic algorithms in pre-stressing simulations requiring element-level manipulation of the solvers ([Pierce et al., 2015](#); [Weisbecker et al., 2014](#)). The major steps of the new backward scheme are outlined in [Algorithm 2](#).

Algorithm 2. Implementation of the backward algorithm with MO at each point to recover the pre-stress state.

1. Initialize the parameters of the backward and forward models with the *in vivo* data
2. while $\text{maximum}(r) > \epsilon$ do:
3. Perform a forward analysis by imposing the pre-stress σ_0 into the current state \mathbf{V} of the model to find the updated state of the isotropic material variables and coordinates \mathbf{v}_R
4. Perform an inverse analysis with mapping $\mathbf{X}^{REF} \mapsto \mathbf{x}$ using the boundary conditions to find the updated state of the anisotropic material parameters \mathbf{v}_A
5. For each point do:
6. $\mathbf{U}_R \leftarrow \mathbf{V}_R^{REF} - \mathbf{v}_R$
7. $\mathbf{V}_R \leftarrow \mathbf{V}_R + \mathbf{U}_R$
8. $\mathbf{v} \leftarrow \mathbf{v}_R \cup \mathbf{v}_{ANI}$
9. $r \leftarrow \|\mathbf{v} - \mathbf{V}^{REF}\|_2$
10. end for
11. end while

2.3. Abaqus implementation

The soils consolidation theory in Abaqus (Dassault Systèmes, 2019) was used for solving the FE analysis by eq. (3) such that in each forward analysis of pre-stress in AC, the stress-free values of the material parameters of the mixture model can be implemented by a custom Fortran SDVINI subroutine, which assigns the initial values of the state variables for each integration point of the FE model, following step 0, which calculates the geometrical parameters of these points. Therefore, any material parameters can be initialized heterogeneously, and the

calculated variables can then be passed to the Fortran UMAT subroutine, which was called for the implementation of the solid parts of the tissue within Abaqus by eq. (4) (see Fig. 3). Further information about the implementation of the material model and its parameters is presented in the article of Sajjadinia et al. (2019).

To implement the backward optimization algorithm, a custom Python script was implemented in Abaqus, according to Algorithm 2, where first, two identical FE models were created based on the initial *in vivo* data for the forward and inverse analyses. Subsequently, all the *in vivo* boundary conditions were prescribed in both models, while the inverse model should also have the displacement boundary conditions on all of its nodes with the initial value of zero, showing the undeformed

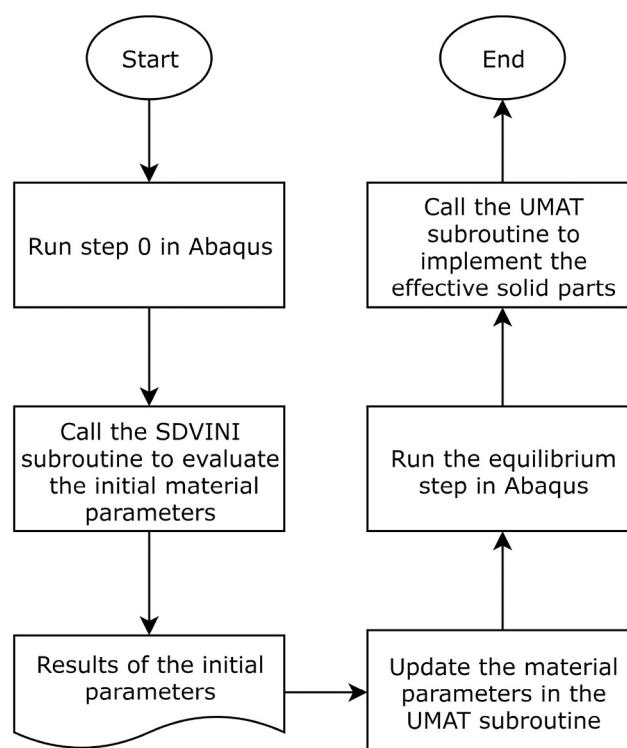


Fig. 3. Flowchart of the implementation of pre-stressing equilibrium in AC mixture models with initial conditions passed to Abaqus by a Fortran subroutine.

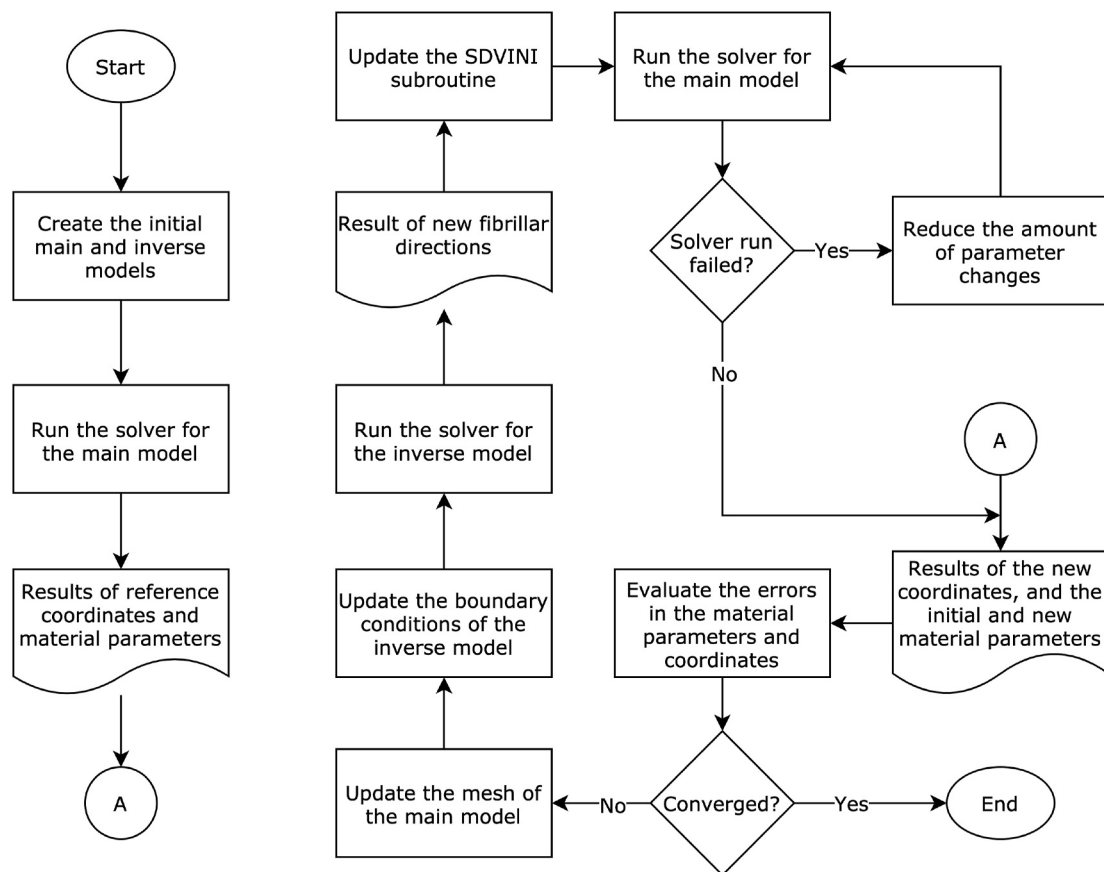


Fig. 4. Flowchart of the backward optimization with MO implemented in Abaqus by a custom Python code.

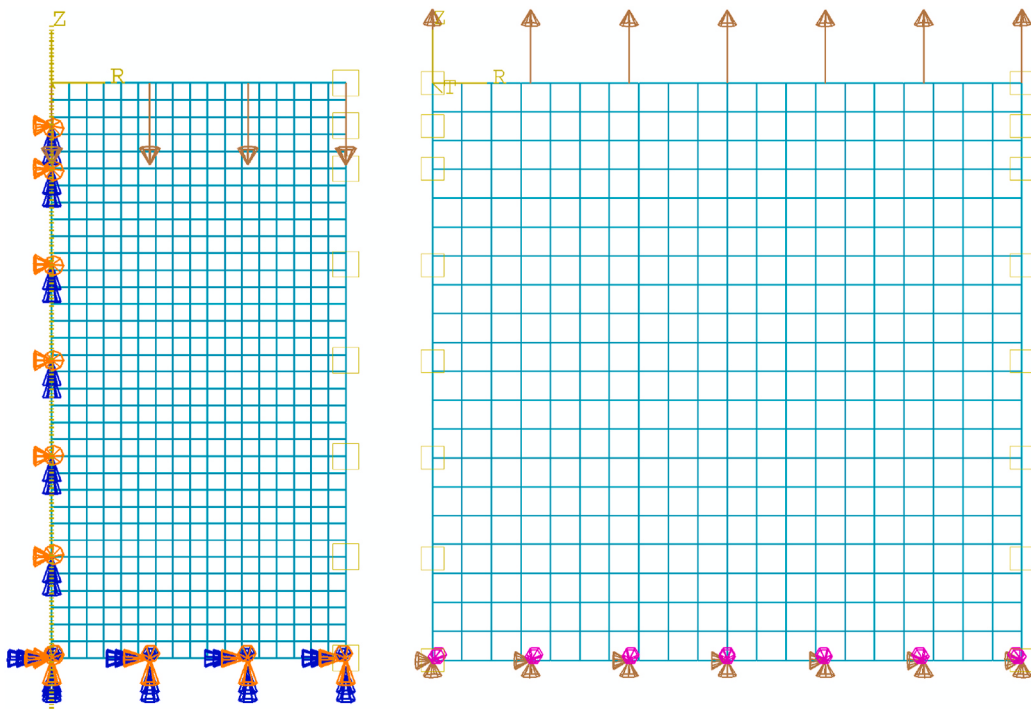


Fig. 5. 2D FE models include an axisymmetric mesh (left) and a plane strain mesh (right).

condition. For implementation of the backward algorithm, the material parameters at each integration point and the nodal geometrical parameters, forming the state variables, can be extracted from a forward analysis of the pre-stress equilibrium.

Afterward, the backward algorithm could be implemented in a loop, which first evaluates the errors in the state variables and then, as documented in [Algorithm 2](#), the mesh of the forward model and the final values of the nodal boundary conditions of the inverse model are updated. Upon running the backward analysis, the anisotropic parameters can be identified by eq. (8), while the other state variables can be extracted from the final values of the results of the forward analysis. The new values of the isotropic material parameters can be identified using eq. (9), which then may be implemented by updating the SDVINI subroutine to implement another iteration of this loop with the new state variables. This backward algorithm continued until convergence; nonetheless, at some iterations, the high amount of variations in the state variables might lead to failures in solving the FE problems, which can be handled by decreasing the updates of those parameters at the expense of increasing the number of iterations. [Fig. 4](#) summarizes the flowchart of the backward algorithm with MO in Abaqus.

2.4. Simulations

We first assumed that the change in the pre-stress affects mainly the fibrillar part of AC, which is consistent with the previous AC pre-stressing study of [Wang et al. \(2018\)](#). Consequently, a tensile test was simulated with and without MO using 400 8-node biquadratic displacement and bilinear pore pressure elements with full integration by assigning the velocity boundary conditions simulating a stretch of 1.2 at 4000 sec ([Fig. 5](#), right). For this optimization test, a least-squares algorithm was implemented in SciPy to fit the FE models with different fibrillar parameters to the experimental data ([Elliott et al., 2002](#)) via the experimental stress and stretch measurements. The concept of experimental parameters in the pre-stressed FE studies is elaborated in the relevant research of [Wang et al. \(2018\)](#).

To explore the importance of MO, the [Algorithms 1](#) and [2](#) were implemented to find the starting points for an unconfined compression test using 1837 8-node axisymmetric quadrilateral, biquadratic displacement and bilinear pore pressure elements, with full integration, in which the nodal displacements at the symmetrical axis were confined in the radial direction ([Fig. 5](#), left). Subsequently, the changes in the material fractions in the axis of symmetry were calculated. In addition, the variations in the directions of the representative primary fibrils were recorded. For the subsequent compression test, an AC plug with 0.5 mm in radius was axially compressed up to 10% strain by the velocity boundary conditions on the top nodes, with the magnitudes of 0.002 sec⁻¹, which is followed by a relaxation step, where the velocity of the top nodes reduced to zero, while the stress and strain curves were plotted for the outer regions, which are expected to be more influenced by pre-stress than in the inner regions.

Furthermore, in all of the simulations, the AC, modeled with 1 mm thickness, has zero pore pressure on the outer boundaries so that fluid can flow in or out unrestrictedly, and the nodes of the bottom surface of AC were confined in all directions to simulate the osteochondral interface.

Table 1

Fitted material parameters, including the initial elasticity E_0 and strain-dependent elasticity E_e of the fibrillar network for the different pre-stressed models.

Parameter	Result without MO	Result with MO
E_0 (MPa)	30.21	19.51
E_e (MPa)	234.11	230.67

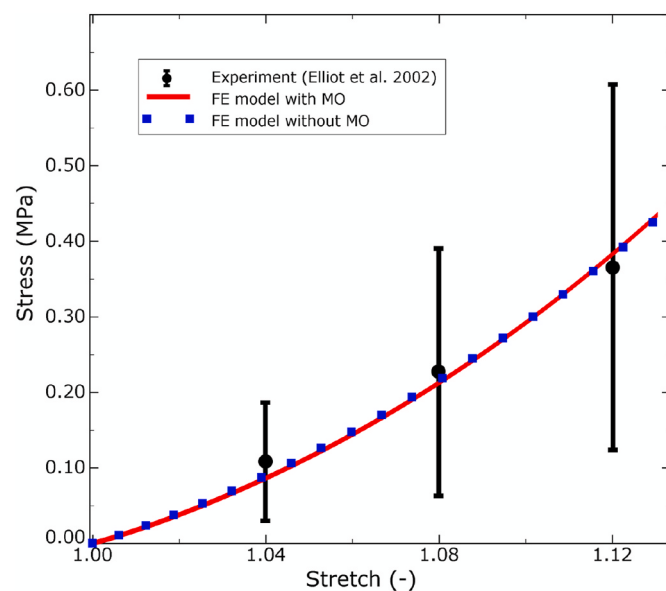


Fig. 6. Stress (in MPa) obtained from experimental data ([Elliott et al., 2002](#)) and from optimized FE models curve-fitted to experimental data as a function of stretch (–).

3. Results

3.1. Tensile test

A set of tensile tests were simulated with and without MO for a wide range of the fibrillar elasticity parameters, with the values of the former research of [Wilson et al. \(2007\)](#), used as an initial guess. [Table 1](#) lists the determined values for both cases, and [Fig. 6](#) represents the simulation results in comparison to experimental data ([Elliott et al., 2002](#)). Both of the FE models fitted similarly to the median values: At first, the recorded stress-strain curves demonstrate a mild nonlinearity due to the initially almost linear behavior of the cartilage, and the curves underestimate the stress in comparison to the median experimental values. Once they reach the middle stretch (around a value of 1.06), the response is dominated by the nonlinear fibrillar elasticity causing a slight overestimation of the stress. Despite this, the recorded responses are still within the range of the experimental data ([Elliott et al., 2002](#)), demonstrating that they both can fit well to the recorded experimental data, which is sufficient for a general AC model.

3.2. Compression test

With the calibrated material models, the backward FE simulations were also carried out in the confined compression test with and without MO, and the stress-free states were found. Both of the models converged well, although the model with MO required more iterations in order to reach convergence.

[Fig. 7](#) presents the contours of the angle θ between the radial axis and the representative primary fibril direction in each point upon reaching the equilibrium condition. The model with MO fitted completely to the *in vivo* data ([Fig. 1](#)), whereas the model without MO showed some changes in the angles ranging from 5 to 10% relative to the *in vivo* data in the periphery regions. In the axis of symmetry, however, the fibrils did not rotate as their elements in this axis are radially confined due to the model symmetry. Note that, at the right bottom corner of the AC model, a local change in values is observable, which can also be correlated to the extreme rotation of the element in that region, it may also be affected by numerical errors, and therefore, its variation is disregarded in this study.

[Fig. 8](#) illustrates the changes in the material volume fractions in

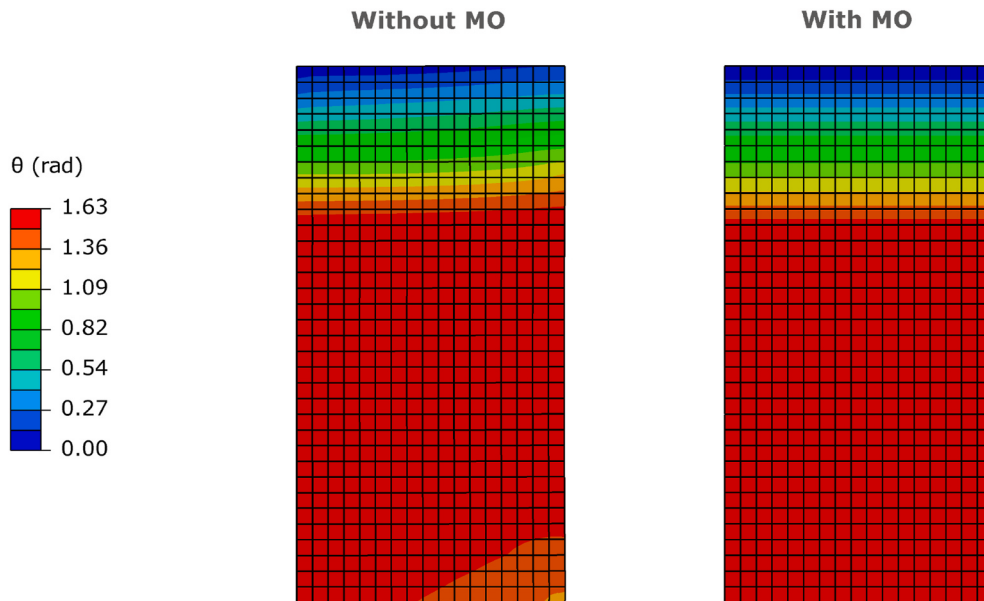


Fig. 7. Contour plots of the angle θ (rad) between the radial axis and the representative primary fibril in the initial condition after equilibrium with and without MO.

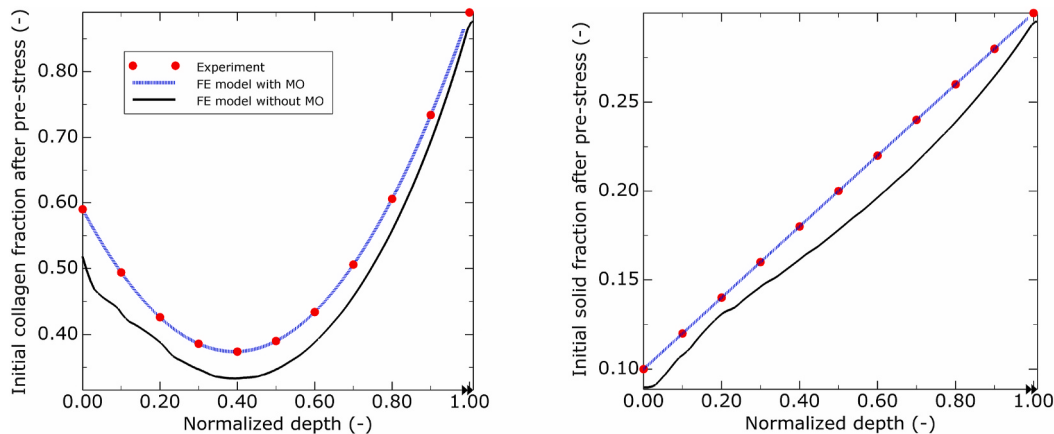


Fig. 8. Plots of volume fractions (–) vs normalized depth (–) of cartilage in the initial condition after equilibrium for *in vivo* data (Lipshitz et al., 1975; Rieppo, 2004; Shapiro et al., 2001; Wilson et al., 2007) together with the results of FE models with and without MO.

terms of the normalized depth in the axis of symmetry of the cartilage. Although both models present similar trends, the model without MO recorded roughly between 8 and 16% variations with respect to the experimental data for most regions, while in the deeper zones they both converged to similar values.

Next, the model underwent the compression test with and without MO, and the axial stress-strain curves of the effective solid components were extracted in the middle of each AC zone (Fig. 9), representing the significant changes in all AC layers, i.e. the superficial zone (SZ), the middle zone (MZ) and the deep zone (DZ). At the peak load, the fibrillar part shows a maximum variation of 44% in the stress response, where in MZ, the fibrillar stress increased from 0.42 to 0.71 MPa when the MO algorithm was employed. In SZ and DZ, these variations in the fibrillar stresses, due to application of the MO algorithm, were respectively 9% and 12%. For the other components of the solid parts, the maximum variation of the stress corresponds to the non-fibrillar part with around 16% of alteration in its magnitude.

Comparatively, MO affected less the total stress-strain curves of different AC zones, as displaced in Fig. 10; nonetheless, the MO effect in DZ is more discernible, particularly during relaxation, where approximately 12% variation in the magnitudes of the strains is observable. The

variations in the other two zones are less than 9%.

4. Discussion

In the present paper, a new and efficient backward optimization algorithm was proposed encompassing nodal geometrical optimization together with MO for FE analysis of an anisotropic and depth-dependent mixture model of AC consisting of fibrillar, non-fibrillar, GAG, and fluid constituents. Our MO method can overcome the theoretical inconsistency with the *in vivo* and numerically pre-stressed states of the material parameters of the AC mixture models by incorporating the material variables into the convergence criteria of a previous backward algorithm (Bols et al., 2013; Pandolfi and Holzapfel, 2008; Wang et al., 2018), and implementing an inverse version of the forward model for the parameters capturing anisotropy. Therefore, we hypothesized that the heterogeneous material properties of the AC mixture model can be altered if the backward FE analysis is used with MO, which can subsequently affect the mechanical tissue responses.

At first, a number of curve-fitting tensile tests were simulated, analogous to a recent pre-stressing study (Wang et al., 2018), to determine the effect of MO algorithms on the final calibrated values of the

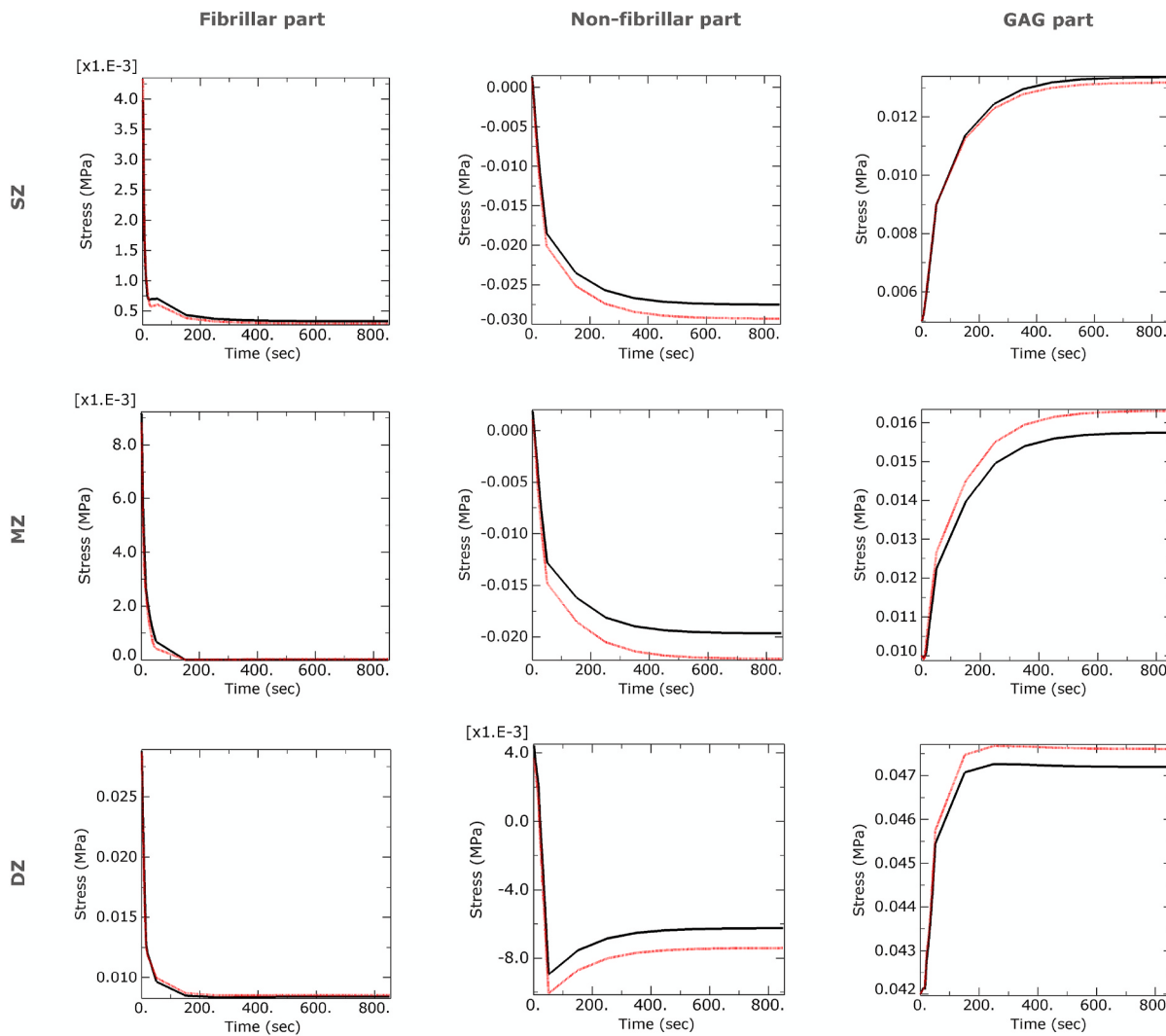


Fig. 9. Plots of stress (MPa) vs time (sec) for FE simulations of unconfined compression tests with MO (black curves) and without MO (red curves) for different AC zones (SZ = superficial zone; MZ = middle zone; DZ = deep zone), and for different parts of the AC effective stresses after equilibrium.

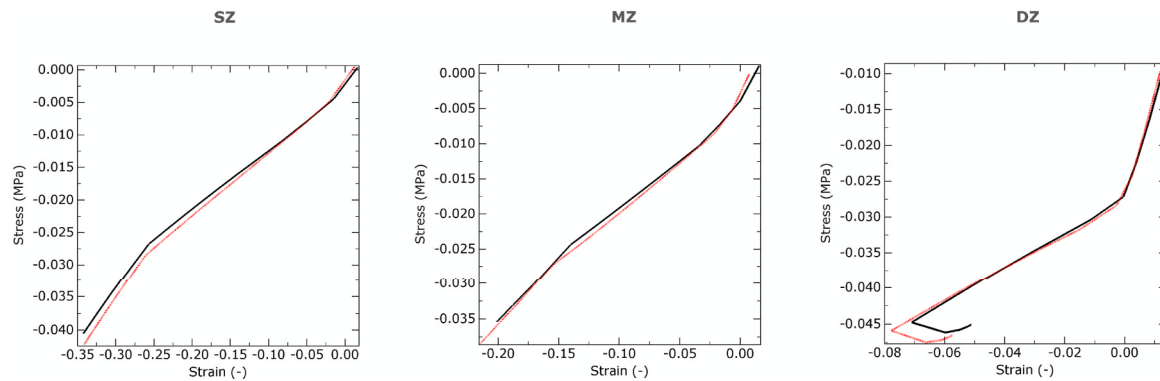


Fig. 10. Plots of total stress (MPa) vs strain (-) for FE simulations of unconfined compression tests with MO (black curves) and without MO (red curves) for different AC zones (SZ = superficial zone; MZ = middle zone; DZ = deep zone).

fibrillar parameters, considering that the validated constitutive equations used in this study had not been implemented with any of the pre-stressing methods. The results of this test show that while both calibrated models could respond within the range of experimental data (Elliott et al., 2002) (Fig. 6), the model without MO has a slightly more strain-dependent fibrillar elasticity but considerably greater initial

elasticity. This can be explained by the fact that at the initial pre-stressing condition, most of the osmotic pressure is resisted by the fibrillar network (Quiroga et al., 2017), and also, considering that the model without MO has reduced solid and collagen fractions, according to eq. (9), the fibrillar elasticity should be increased to compensate for it, especially the initial fibrillar elasticity, which is the dominating material

parameter at small strains.

Next, to test the hypothesis, a multiphasic cartilage material model (Sajjadinia et al., 2019) was implemented in the representative unconfined compression test with MO and without MO for the sake of comparison. When the backward model without MO was implemented, the errors in the fibrillar directions (Fig. 7) and the considerable errors in the material parameters (Fig. 8), support our hypothesis, as they can affect the mechanical response by eqs. (8) and (9). In addition, the previous study of Julkunen et al. (2008) reported that the change in the solid and collagen fractions can highly affect the mechanical responses, while keeping their trends. Therefore, these results indirectly validate the higher accuracy and importance of the MO algorithm. We further clarify the change in the mechanical responses by simulating subsequent relaxation tests.

When MO was used, the calculated stresses in the relaxation test changed significantly in comparison to the results of the conventional backward algorithm (Fig. 9), which unveils the role that MO can play in the mechanical response of the tissue, and again supports our hypothesis. However, both of the models resulted in similar trends in conformity with the previous observations, where, e.g., the osmotic pressure contributed most to the load resistance, similar to former findings (Quiroga et al., 2017). In addition, the fibrillar parts started in all regions with a high value of stress magnitudes and then equilibrated with negligible values, as observed in a previous depth-dependent study (Wilson et al., 2007). The recorded stress in DZ for the fibrillar network is greatly more than other regions, considering that osmotic pressure is higher in this region, and also the primary fibrils are oriented mostly axially and consequently contributed more to the axial load resistance due to initial pre-stress, whereas the fibrils in the upper regions tend to be aligned radially.

In terms of the total stress-strain curves, both algorithms again led to similar trends across different AC zones (Fig. 10), although the results show a small but notable change especially in the relaxation stage, where the change in the volumes of the elements increased the influence of the errors in the volume fractions.

Overall, the analogous trends in the results demonstrate the comparable fidelity in both methods, but it can still be of importance for some highly-personalized or accurate models, considering that in the future such multiphasic studies are moving towards more exact and realistic FE analysis of the AC model with precise image-based data of the diverse phases (Klika et al., 2016), in which the pre-stressing inaccuracy might be of importance, e.g., for patient-specific studies (Linka et al., 2017; Meng et al., 2016; Pierce et al., 2010) or the damage models correlate with these stress-strain data (Eskelinen et al., 2019; Hosseini et al., 2014; Liu et al., 2019; Mononen et al., 2016; Stender et al., 2016).

The present study has some limitations. Firstly, the material model was calibrated using a single type of tensile test in keeping with the validation test of a previous similar study (Wang et al., 2018) to roughly capture the effect of the new algorithm on the parameters. While this is not a major limitation, as this study was not designed to determine an exact AC model, we acknowledge that our general AC model can merely simulate the general behavior of tissues, as we have needed in the comparative tests. Moreover, the MO method was only tested on a particular healthy AC model, and its applicability in the analysis of the other models, such as softer degenerated cartilage samples (Robinson et al., 2016), is not guaranteed, because they are prone to excessive distortions. In this case, the MO should be updated by an algorithm that can eliminate the distortions (Maas et al., 2016) or can optimize the alterations in each iteration (Rausch et al., 2017).

In conclusion, our backward optimization algorithm provides a new and pragmatic computational framework for the implementation of anisotropic and heterogeneous AC mixture models with the initial *in vivo* state of both material and geometrical parameters. The comparative study could elucidate the importance of the proposed MO method in the stress analysis of the AC components with pre-stress. This method, which is applicable in most of the FE solvers, can be implemented in future

image-based biomechanical modeling and damage studies, where high accuracies in the prediction of the mechanical responses of the mixture models are of concern.

CRediT authorship contribution statement

Seyed Shayan Sajjadinia: Conceptualization, Methodology, Investigation, Software, Formal analysis, Writing - original draft, Validation, Writing - review & editing. **Bruno Carpentieri:** Supervision, Writing - original draft. **Gerhard A. Holzapfel:** Supervision, Writing - review & editing.

Declaration of competing interest

The authors declare that they have no known competing financial interests or personal relationships that could have appeared to influence the work reported in this paper.

Acknowledgement

This work was supported by the Open Access Publishing Fund of the Free University of Bozen-Bolzano.

References

- Alastrué, V., García, A., Peña, E., Rodríguez, J.F., Martínez, M.A., Doblaré, M., 2010. Numerical framework for patient-specific computational modelling of vascular tissue. *Int. j. numer. method. biomed. eng.* 26, 35–51. <https://doi.org/10.1002/cnm.1234>.
- Alastrué, V., Peña, E., Martínez, M.Á., Doblaré, M., 2007. Assessing the use of the “opening angle method” to enforce residual stresses in patient-specific arteries. *Ann. Biomed. Eng.* 35, 1821–1837. <https://doi.org/10.1007/s10439-007-9352-4>.
- Ambrosi, D., Amar, M. Ben, Cyron, C.J., DeSimone, A., Goriely, A., Humphrey, J.D., Kuhl, E., 2019. Growth and remodelling of living tissues: perspectives, challenges and opportunities. *J. R. Soc. Interface* 16. <https://doi.org/10.1098/rsif.2019.0233>.
- Benninghoff, A., 1925. Form und Bau der Gelenkknorpel in ihren Beziehungen zur Funktion. *Z. Anat. Entwicklungsgesch.* 76, 43–63. <https://doi.org/10.1007/BF02134417>.
- Bols, J., Degroot, J., Trachet, B., Verhegge, B., Segers, P., Vierendeels, J., 2013. A computational method to assess the *in vivo* stresses and unloaded configuration of patient-specific blood vessels. *J. Comput. Appl. Math.* 246, 10–17. <https://doi.org/10.1016/j.cam.2012.10.034>.
- Buschmann, M.D., Grodzinsky, A.J., 1995. A molecular model of proteoglycan-associated electrostatic forces in cartilage mechanics. *J. Biomech. Eng.* 117, 179–192. <https://doi.org/10.1115/1.2796000>.
- Dassault Systèmes, 2019. SIMULIA Abaqus.
- Elliott, D.M., Narmoneva, D.A., Setton, L.A., 2002. Direct measurement of the Poisson's ratio of human patella cartilage in tension. *J. Biomech. Eng.* 124, 223–228. <https://doi.org/10.1115/1.1449905>.
- Eskelinen, A.S.A., Mononen, M.E., Venäläinen, M.S., Korhonen, R.K., Tanska, P., 2019. Maximum shear strain-based algorithm can predict proteoglycan loss in damaged articular cartilage. *Biomech. Model. Mechanobiol.* 18, 753–778. <https://doi.org/10.1007/s10237-018-01113-1>.
- Fachinotti, V.D., Cardona, A., Jetteur, P., 2008. Finite element modelling of inverse design problems in large deformations anisotropic hyperelasticity. *Int. J. Numer. Methods Eng.* 74, 894–910. <https://doi.org/10.1002/nme.2193>.
- Freutel, M., Schmidt, H., Dürselen, L., Ignatius, A., Galbusera, F., 2014. Finite element modeling of soft tissues: material models, tissue interaction and challenges. *Clin. Biomech.* 29, 363–372. <https://doi.org/10.1016/j.clinbiomech.2014.01.006>.
- Gee, M.W., Förster, C., Wall, W.A., 2010. A computational strategy for prestressing patient-specific biomechanical problems under finite deformation. *Int. J. Numer. Method. Biomed. Eng.* 26, 52–72. <https://doi.org/10.1002/cnm.1236>.
- Govindjee, S., Mihalic, P.A., 1996. Computational methods for inverse finite elastostatics. *Comput. Methods Appl. Mech. Eng.* 136, 47–57. [https://doi.org/10.1016/0045-7825\(96\)01045-6](https://doi.org/10.1016/0045-7825(96)01045-6).
- Grytz, R., Downs, J.C., 2013. A forward incremental prestressing method with application to inverse parameter estimations and eye-specific simulations of posterior scleral shells. *Comput. Methods Biomed. Eng.* 16, 768–780. <https://doi.org/10.1080/10255842.2011.641119>.
- Halloran, J.P., Sibole, S., Van Donkelaar, C.C., Van Turnhout, M.C., Oomens, C.W.J.J., Weiss, J.A., Guilak, F., Erdemir, A., 2012. Multiscale mechanics of articular cartilage: potentials and challenges of coupling musculoskeletal, joint, and microscale computational models. *Ann. Biomed. Eng.* 40, 2456–2474. <https://doi.org/10.1007/s10439-012-0598-0>.
- Hosseini, S.M., Wilson, W., Ito, K., Van Donkelaar, C.C., 2014. A numerical model to study mechanically induced initiation and progression of damage in articular cartilage. *Osteoarthritis Cartilage* 22, 95–103. <https://doi.org/10.1016/j.joca.2013.10.010>.

- Huang, Y., Teng, Z., Elkawad, M., Tarkin, J.M., Joshi, N., Boyle, J.R., Buscombe, J.R., Fryer, T.D., Zhang, Y., Park, A.Y., Wilkinson, I.B., Newby, D.E., Gillard, J.H., Rudd, J.H.F., 2016. High structural stress and presence of intraluminal thrombus predict abdominal aortic aneurysm 18F-FDG uptake: insights from biomechanics. *Circ. Cardiovasc. Imaging* 9, 1–9. <https://doi.org/10.1161/CIRCIMAGING.116.004656>.
- Julkunen, P., Wilson, W., Isaksson, H., Jurvelin, J.S., Herzog, W., Korhonen, R.K., 2013. A review of the combination of experimental measurements and fibril-reinforced modeling for investigation of articular cartilage and chondrocyte response to loading. *Comput. Math. Methods Med.* 2013 326150. <https://doi.org/10.1155/2013/326150>.
- Julkunen, P., Wilson, W., Jurvelin, J.S., Rieppo, J., Qu, C.J., Lammi, M.J., Korhonen, R.K., 2008. Stress-relaxation of human patellar articular cartilage in unconfined compression: prediction of mechanical response by tissue composition and structure. *J. Biomech.* 41, 1978–1986. <https://doi.org/10.1016/j.jbiomech.2008.03.026>.
- Klika, V., Gaffney, E.A., Chen, Y.C., Brown, C.P., 2016. An overview of multiphase cartilage mechanical modelling and its role in understanding function and pathology. *J. Mech. Behav. Biomed. Mater.* 62, 139–157. <https://doi.org/10.1016/j.jmbbm.2016.04.032>.
- Leach, J.R., Zhu, C., Saloner, D., Hope, M.D., 2019. Comparison of two methods for estimating the unloaded state for abdominal aortic aneurysm stress calculations. *J. Mech. Med. Biol.* 19, 1950015. <https://doi.org/10.1142/S0219519419500155>.
- Linka, K., Itskov, M., Truhn, D., Nebelung, S., Thüring, J., 2017. T2 MR imaging vs. computational modeling of human articular cartilage tissue functionality. *J. Mech. Behav. Biomed. Mater.* 74, 477–487. <https://doi.org/10.1016/j.jmbbm.2017.07.023>.
- Lipshitz, H., Etheredge, R., Glimcher, M., 1975. In vitro wear of articular cartilage. *J. Bone Jt. Surg.* 57, 527–534. <https://doi.org/10.2106/00004623-197557040-00015>.
- Liu, D., Ma, S., Stoffel, M., Markert, B., 2019. A biphasic visco-hyperelastic damage model for articular cartilage: application to micromechanical modelling of the osteoarthritis-induced degradation behaviour. *Biomech. Model. Mechanobiol.* 19, 1055–1077. <https://doi.org/10.1007/s10237-019-01270-x>.
- Lu, J., Zhou, X., Raghavan, M.L., 2007. Inverse elastostatic stress analysis in pre-deformed biological structures: demonstration using abdominal aortic aneurysms. *J. Biomech.* 40, 693–696. <https://doi.org/10.1016/j.jbiomech.2006.01.015>.
- Maas, S.A., Erdemir, A., Halloran, J.P., Weiss, J.A., 2016. A general framework for application of prestrain to computational models of biological materials. *J. Mech. Behav. Biomed. Mater.* 61, 499–510. <https://doi.org/10.1016/j.jmbbm.2016.04.012>.
- Meng, Q., An, S., Damion, R.A., Jin, Z., Wilcox, R., Fisher, J., Jones, A., 2016. The effect of collagen fibril orientation on the biphasic mechanics of articular cartilage. *J. Mech. Behav. Biomed. Mater.* 65, 439–453. <https://doi.org/10.1016/j.jmbbm.2016.09.001>.
- Mononen, M.E., Tanska, P., Isaksson, H., Korhonen, R.K., 2016. A novel method to simulate the progression of collagen degeneration of cartilage in the knee: data from the osteoarthritis initiative. *Sci. Rep.* 6, 21415. <https://doi.org/10.1038/srep21415>.
- Mow, V.C., Kuei, S.C., Lai, W.M., Armstrong, C.G., 1980. Biphasic creep and stress relaxation of articular cartilage in compression: theory and experiments. *J. Biomech. Eng.* 102, 73–84. <https://doi.org/10.1115/1.3138202>.
- Olsson, T., Stålhund, J., Klarbring, A., 2006. Modeling initial strain distribution in soft tissues with application to arteries. *Biomech. Model. Mechanobiol.* 5, 27–38. <https://doi.org/10.1007/s10237-005-0008-8>.
- Pandolfi, A., Holzapfel, G.A., 2008. Three-dimensional modeling and computational analysis of the human cornea considering distributed collagen fibril orientations. *J. Biomech. Eng.* 130, 061006 <https://doi.org/10.1115/1.2982251>.
- Pierce, D.M., Fastl, T.E., Rodriguez-Vila, B., Verbrugge, P., Fourneau, I., Maleux, G., Herijgers, P., Gomez, E.J., Holzapfel, G.A., 2015. A method for incorporating three-dimensional residual stretches/stresses into patient-specific finite element simulations of arteries. *J. Mech. Behav. Biomed. Mater.* 47, 147–164. <https://doi.org/10.1016/j.jmbbm.2015.03.024>.
- Pierce, D.M., Trobin, W., Raya, J.G., Trattnig, S., Bischof, H., Glaser, C., Holzapfel, G.A., 2010. DT-MRI based computation of collagen fiber deformation in human articular cartilage: a feasibility study. *Ann. Biomed. Eng.* 38, 2447–2463. <https://doi.org/10.1007/s10439-010-9990-9>.
- Quiroga, J.M.P.P., Wilson, W., Ito, K., van Donkelaar, C.C., 2017. Relative contribution of articular cartilage's constitutive components to load support depending on strain rate. *Biomech. Model. Mechanobiol.* 16, 151–158. <https://doi.org/10.1007/s10237-016-0807-0>.
- Rausch, M.K., Genet, M., Humphrey, J.D., 2017. An augmented iterative method for identifying a stress-free reference configuration in image-based biomechanical modeling. *J. Biomech.* 58, 227–231. <https://doi.org/10.1016/j.jbiomech.2017.04.021>.
- Rieppo, J., 2004. Spatial determination of water, collagen and proteoglycan content by Fourier transform infrared imaging and digital tensitometry. *50th Annu. Meet. Orthop. Res. Soc. Poster No 1021*.
- Robinson, D.L., Kersh, M.E., Walsh, N.C., Ackland, D.C., de Steiger, R.N., Pandy, M.G., 2016. Mechanical properties of normal and osteoarthritic human articular cartilage. *J. Mech. Behav. Biomed. Mater.* 61, 96–109. <https://doi.org/10.1016/j.jmbbm.2016.01.015>.
- Sajjadinia, S.S., Haghpanahi, M., Razi, M., 2019. Computational simulation of the multiphasic degeneration of the bone-cartilage unit during osteoarthritis via indentation and unconfined compression tests. *Proc. Inst. Mech. Eng. Part H J. Eng. Med.* 233, 871–882. <https://doi.org/10.1177/0954411919854011>.
- Shapiro, E.M., Borthakur, A., Kaufman, J.H., Leigh, J.S., Reddy, R., 2001. Water distribution patterns inside bovine articular cartilage as visualized by 1H magnetic resonance imaging. *Osteoarthritis Cartilage* 9, 533–538. <https://doi.org/10.1053/joca.2001.0428>.
- Stender, M.E., Carpenter, R.D., Regueiro, R.A., Ferguson, V.L., 2016. An evolutionary model of osteoarthritis including articular cartilage damage, and bone remodeling in a computational study. *J. Biomech.* 49, 3502–3508. <https://doi.org/10.1016/j.jbiomech.2016.09.024>.
- Stender, M.E., Raub, C.B., Yamauchi, K.A., Shirazi, R., Vena, P., Sah, R.L., Hazelwood, S.J., Klisch, S.M., 2012. Integrating qPLM and biomechanical test data with an anisotropic fiber distribution model and predictions of TGF- β 1 and IGF-1 regulation of articular cartilage fiber modulus. *Biomech. Model. Mechanobiol.* 12, 1073–1088. <https://doi.org/10.1007/s10237-012-0463-y>.
- Taffetani, M., Griebel, M., Gastaldi, D., Klisch, S.M., Vena, P., 2014. Poroviscoelastic finite element model including continuous fiber distribution for the simulation of nanoindentation tests on articular cartilage. *J. Mech. Behav. Biomed. Mater.* 32, 17–30. <https://doi.org/10.1016/j.jmbbm.2013.12.003>.
- Truesdell, C., Toupin, R., 1960. The classical field theories. In: Flügge, S. (Ed.), *Principles of Classical Mechanics and Field Theory/Prinzipien der klassischen Mechanik und Feldtheorie*. Springer Berlin Heidelberg, Berlin, Heidelberg, pp. 226–858. https://doi.org/10.1007/978-3-642-45943-6_2.
- Wang, X., Eriksson, T.S.E., Ricken, T., Pierce, D.M., 2018. On incorporating osmotic prestretch/prestress in image-driven finite element simulations of cartilage. *J. Mech. Behav. Biomed. Mater.* 86, 409–422. <https://doi.org/10.1016/j.jmbbm.2018.06.014>.
- Weisbecker, H., Pierce, D.M., Holzapfel, G.A., 2014. A generalized prestressing algorithm for finite element simulations of preloaded geometries with application to the aorta. *Int. J. Numer. Method. Biomed. Eng.* 30, 857–872. <https://doi.org/10.1002/cnm.2632>.
- Wilson, W., Huyghe, J.M., Van Donkelaar, C.C., 2007. Depth-dependent compressive equilibrium properties of articular cartilage explained by its composition. *Biomech. Model. Mechanobiol.* 6, 43–53. <https://doi.org/10.1007/s10237-006-0044-z>.
- Wilson, W., van Donkelaar, C.C., van Rietbergen, B., Ito, K., Huiskes, R., 2004. Stresses in the local collagen network of articular cartilage: a poroviscoelastic-fibril-reinforced finite element study. *J. Biomech.* 37, 357–366. [https://doi.org/10.1016/S0021-9290\(03\)00267-7](https://doi.org/10.1016/S0021-9290(03)00267-7).
- Wu, J.Z., Herzog, W., 2000. Finite element simulation of location- and time-dependent mechanical behavior of chondrocytes in unconfined compression tests. *Ann. Biomed. Eng.* 28, 318–330. <https://doi.org/10.1114/1.271>.
- Zahn, A., Balzani, D., 2016. Modeling of anisotropic growth and residual stresses in arterial walls. *Acta Polytech. CTU Proc.* 7, 85. <https://doi.org/10.14311/app.2017.7.0085>.